Sedimentation Studies on the Kinesin Motor Domain Constructs K401, K366, and K341[†]

John J. Correia,*[,‡] S. P. Gilbert,[§,||] M. L. Moyer,[§] and K. A. Johnson[§]

Department of Biochemistry, University of Mississippi Medical Center, 2500 North State Street, Jackson, Mississippi 39216, and Department of Biochemistry and Molecular Biology, The Pennsylvania State University, University Park, Pennsylvania 16802

Received December 28, 1994; Revised Manuscript Received February 10, 1995[⊗]

ABSTRACT: Bacterial expressed kinesin motor domains hydrolyze ATP and promote microtubule-dependent motility. It has routinely been assumed that motor domain preparations are monomeric on the basis of the presumption that dimerization is mediated by the stalk region. However, experimental verification of the oligomeric state of the kinesin construct is required to interpret the results from single-molecule motility assays as well as presteady-state kinetic experiments. We have measured directly the state of assembly of three conventional kinesin motor domain constructs—K401, K366, and K341, comprising the N-terminal 401, 366, and 341 amino acids, respectively, of the *Drosophila* kinesin heavy chain—by sedimentation velocity and sedimentation equilibrium methods in an analytical ultracentrifuge. K401 (MW of ADP complex, 45 532) is a predominantly a dimer with a sedimentation coefficient, $s^0_{20,w}$, of 5.06 S, but it is able to self-associate by means of a 1−2−4 mechanism into higher oligomers. Molecular weight measurements establish the dissociation constant for dimerization at 37 ± 17 nM in the presence of ATP. The dissociation constant in the presence of ADP is 35 ± 26 nM and in the presence of AMPPNP is 42 ± 28 nM. The construct K366 (MW of ADP complex, 41 404) is a monomer (measured MW, 41 768 ± 1219) at concentrations below 4 μM K366, with a sedimentation coefficient, $s^0_{20,w}$, of 3.25 S. At higher concentrations, there is evidence for a weak association of K366 to a 1−2−4−8 model with a slight preference for octamer formation. The smallest construct, K341 (MW of ADP complex, 38 274), is a monomer (measured MW, 38 191 ± 734) up to at least 10 μM total K341 concentration with a sedimentation coefficient, $s^0_{20,w}$, of 2.9 S. Thus, the dimerization domain either is between amino acid residues 367 and 401 or is strongly affected by the removal of this region. Higher oligomers of K401 form by a mechanism involving dimers of dimers, and suggest that native kinesin may also undergo self-association. These results have important implications for the interpretation of ATP-dependent motility assays.

Kinesin is a microtubule-dependent ATPase involved in the movement of axoplasmic organelles toward the synapse (Gho et al., 1992). Since kinesin's discovery in 1985, investigators have been fascinated by its motility as observed by video-enhanced light microscopy (Allen et al., 1985; Lasek & Brady, 1985; Vale et al., 1985a,b; Porter et al., 1987). Kinesin promotes plus-end-directed microtubule translocations in vitro, observed either as microtubule gliding on coverslips adsorbed with kinesin or as kinesin-coated bead movements along microtubules. These assays have permitted the determination of the translocation velocity, step size (distance moved per ATP), and force produced by single and multiple kinesins (Berliner et al., 1984, 1995; Stewart et al., 1993; Romberg & Vale, 1993; Howard et al., 1989; Cohn et al., 1989; Yang et al., 1990; Svoboda et al., 1993; Kuo & Sheetz, 1993; Svoboda & Block, 1994; Hunt et al., 1994). In addition, motility experiments have revealed that a single molecule of kinesin (dimeric with two motor domains) will promote translocations along the microtubule at a maximum velocity (Howard et al., 1989; Block et al., 1990; Romberg & Vale, 1993). The tendency of kinesin to track single protofilaments (Gelles et al., 1988; Ray et al., 1993) and to translocate along the microtubule for long distances has led to the designation of kinesin as a highly "processive enzyme" in comparison to skeletal myosin. In contrast to kinesin, multiple myosin molecules are required for directed movements along actin filaments, and as the number of myosin molecules is increased, the speed of translocation increases (Uyeda et al., 1991). Native kinesin contains two motor domains connected by an α-helical coiled coil stalk (Hirokawa et al., 1989; Yang et al., 1989; de Cuevas et al., 1992). The motor domain has been defined as the N-terminal 340−450 amino acids of the kinesin heavy chain polypeptide (Yang et al., 1990; Stewart et al., 1993), and truncated polypeptides expressed in *Escherichia coli* demonstrate a microtubule-activated ATPase, promote microtubule-based movements, and generate force (Yang et al., 1990; Stewart et al., 1993; Berliner et al., 1994; Gilbert & Johnson, 1993, 1994; Huang & Hackney, 1994; Huang et al., 1994). In addition, one of these constructs, K401 (N-terminal 401 amino acids) has been shown to exhibit the kinetic characteristics of native kinesin (Gilbert & Johnson,

[†] This work was supported by Research Grants GM41117 (J.J.C.), BIR-9216150 (J.J.C.), and GM26726 (K.A.J.).

* To whom correspondence should be addressed: Department of Biochemistry, University of Mississippi Medical Center, 2500 North State Street, Jackson, MS 39216. (601) 984-1522; fax (601) 984-1501.

[‡] University of Mississippi Medical Center.

[§] The Pennsylvania State University.

[||] Current address: Department of Biological Sciences, 215A Clapp Hall, University of Pittsburgh, Pittsburgh, PA 15260.

[⊗] Abstract published in *Advance ACS Abstracts,* April 1, 1995.

0006-2960/95/0434-4898$09.00/0

1993, 1994; Harrison et al., 1993; Gilbert et al., 1995; Berliner et al., 1995). Furthermore, pre-steady-state experiments with K401 have resulted in a mechanism that accounts for the apparent processivity of the kinesin dimer in the motility experiments (Gilbert et al., 1995). The unique characteristics of the mechanism are that kinesin cross bridge release occurs after ATP hydrolysis and that, once kinesin is dissociated, it rapidly rebinds to the microtubule. These kinetic results have provided a mechanistic model to account for the apparent processive motility. However, the processivity needs to be defined biochemically (i.e., the number of ATP molecules hydrolyzed per encounter of a kinesin molecule with the microtubule) and to be understood structurally. As the first step in our analysis, the state of association for three conventional kinesin motor domains, K401, K366, and K341, was evaluated by analytical ultracentrifugation. The results presented here show that K401 is a dimeric kinesin, while K366 and K341 (N-terminal 366 and 341 amino acids, respectively) are monomeric.

EXPERIMENTAL PROCEDURES

Reagents. Salts, ADP, and buffer reagents were purchased from Sigma Chemical Company, ATP was from Pharmacia, and AMPPNP was from Boehringer Mannheim.

Expression and Purification of Constructs. The expression and purification of K401 has been described previously (Gilbert & Johnson, 1993). The smaller constructs, K366 and K341 (N-terminal 366 and 341 amino acids, respectively, of the *Drosophila* kinesin heavy chain), were also subcloned into the pET5b expression vector (Rosenberg et al., 1987; Studier et al., 1990) and transformed into the *E. coli* strain HMS174(DE3). Expression and purification of K366 and K341 were as described for K401 with the following modifications. For the BioRex ion-exchange chromatography, the NaCl gradient for K366 was 150 to 500 mM NaCl with the peak fraction eluting at 400 mM NaCl. For K341, the linear gradient was 25 to 500 mM NaCl, and the peak fraction eluted at 300 mM NaCl. The DEAE ion-exchange chromatography was performed with a 10 to 100 mM NaCl linear gradient with the peak fractions of both K341 and K366 eluting at 20 mM NaCl. K401, K341, and K366 were purified in the presence added 20 μM MgATP until the final dialysis step. The added nucleotide appeared to stabilize the activity of the enzyme and increased the yield. K401, K366, and K341 were each purified to homogeneity (>99% by SDS−PAGE).[1] The molecular weight of each protein was calculated on the basis of its amino acid sequence: K401, 45 106; K366, 40 978; K341, 37 848. The protein concentration was determined spectroscopically as described previously (Gilbert & Johnson, 1993), by Bradford assay (1976), and by active site titration (Gilbert & Johnson, 1993).

Analytical Ultracentrifugation. All experiments were conducted on a Beckman Optima XLA analytical ultracentrifuge equipped with absorbance optics and an An60Ti rotor. Temperature was calibrated using 0.1 M $CoCl_2$ in 92.5% ethanol as described by Liu and Stafford (1995). Spectra were integrated from 400 to 750 nm, and total signal was plotted vs temperature. Standard curves were collected on a Gilford Response II and on a Cary 3E spectrophotometer. All experiments were done at a setting of 25 °C, which was found to correspond to 24.6 °C. Sedimentation velocity experiments were all done at 42 000 rpm in charcoal-filled Epon double-sector centerpieces. Velocity data were collected at an appropriate wavelength (230−238 or 280 nm depending upon the initial concentration) and at a spacing of 0.01 cm with four averages in a continuous scan mode. Velocity data were analyzed using XLAVEL (Beckman), SVEDBERG (John Philo, Amgen, Inc.), and DCDT (Walter Stafford, Boston Biomedical Research Institute). XLAVEL differentiates the data to estimate the peak position, r_o, of the absorbance gradient, and plots $\ln(r_o)$ vs $\omega^2 t$ to determine the sedimentation coefficient. SVEDBERG utilizes Faxen's approximation of the Lamm equation to fit the absorbance profiles from a velocity run to sedimentation and diffusion coefficients for up to three noninteracting species (Philo, 1994). For an interacting system that does not resolve into multiple boundaries, for example, a monomer−dimer system (Gilbert, 1959), a single species fit with SVEDBERG is found to be an adequate model (see Results). DCDT generates a distribution of sedimentation coefficients, $g(s)$, by taking the difference of absorbance profiles at successive times, averaged over many differences (Stafford, 1992a,b). The sedimentation coefficients determined with XLAVEL agreed with the determinations by SVEDBERG and corresponded to the peak position in the $g(s)$ profiles. Sedimentation coefficients were corrected to standard conditions, $s_{20,w}$, where indicated (Laue et al., 1992). Equilibrium experiments were performed at 16 000 and 20 000 rpm for K401, at 22 000 rpm for K366, and at 24 000 rpm for K341, in charcoal-filled Epon six-channel centerpieces (Beckman part 331376). Equilibrium data were collected at an appropriate wavelength (230−238 or 280 nm) and at a spacing of 0.001 cm with 16 averages in a step scan mode. Equilibrium was checked by comparing scans at various times up to 24 h. Data sets were edited with REEDIT (Jeff Lary, National Analytical Ultracentrifuge Center, Storrs, CT) to extract the three channels of data and fit individually or jointly with NONLIN (Johnson et al., 1981; PC version provided by Emory Braswell, National Analytical Ultracentrifuge Center, Storrs, CT) to an appropriate association scheme (see Results). NONLIN fits to an effective reduced molecular weight, $\sigma = M(1 - \bar{\nu}\varrho)\omega^2/RT$, where M is the molecular weight, $\bar{\nu}$ is the partial specific volume, ϱ is the solvent density, $\omega = (2\pi(\text{rpm})/60)$, R is the gas constant, and T is the temperature in kelvin (Yphantis & Waugh, 1956). Data from different speeds and from different wavelengths can be combined for global fitting. Fits to a single species give a Z-average σ and thus a Z-average molecular weight, M_z (Lansing & Kraemer, 1935). The sequence-derived molecular weights including one bound nucleotide correspond to the monomer, M_1, in an association scheme. For fits to an association scheme σ_1 was held at the correct value. Equilibrium constants were fit as ln K to contrain them to positive values and were converted from absorbance units to molar units by the appropriate extinction coefficients, corrected for the 1.2-cm path length of the centerpieces and the degree of polymerization, i.e., $K_2 M^{-1} = K_2(\text{abs})^{-1} * (1.2 * \epsilon_1/2)$. (Note: In Nonlin, K_n is, in general, defined as the overall association of n monomers to an n-mer). The extinction coefficients at 280 nm used were 26 740 M^{-1} cm^{-1} for K401, 21 050 M^{-1} cm^{-1} for K366, and 19 770 M^{-1} cm^{-1} for K341 (Gill & von Hippel, 1989). For data collected at other wavelengths, appropriate extinc-

[1] Abbreviations: DTE, dithioerythritol; EDTA, ethylenediaminetetraacetic acid; EGTA, [ethylenebis(oxyethylenenitrilo)]tetraacetic acid; Hepes, 4-(2-hydroxyethyl)-1-piperazineethanesulfonic acid; SDS−PAGE, sodium dodecyl sulfate−polyacrylamide gel electrophoresis.

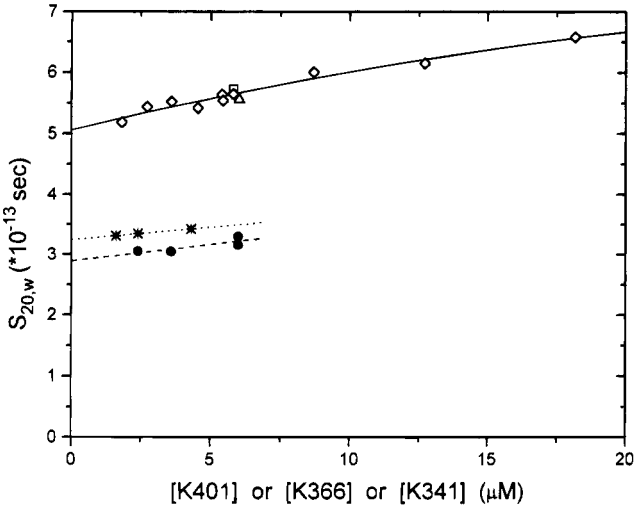

FIGURE 1: Sedimentation coefficient vs protein concentration. The corrected sedimentation coefficient, $s_{20,w}$, is plotted vs the concentration of the kinesin motor domain constructs. Symbols: (◇) K401 + 30 μM ATP, (□) K401 + 30 μM ADP, (△) K401 + 30 μM AMPPNP, (*) K366 + 30 μM ATP, (●) K341 + 30 μM ATP. The lines are linear (K366 and K341) or quadratic (K401) fits to obtain the extrapolated $s^0_{20,w}$ values.

tion coefficients were determined from absorbance values relative to 280 nm. The confidence intervals on parameters estimated by NONLIN were determined by a global search and are presented as error limits (Johnson et al., 1981). For model-independent analysis of equilibrium data, we used an algorithm, BIOSPIN, that does a sliding polynomial fit of the data to extract a local apparent molecular weight (Roark & Yphantis, 1968; Vax version provided by Walter Stafford, Boston Biomedical Research Institute). Nonsuperposition of plots of M_w or M_z vs concentration from different loading concentrations is consistent with sample heterogeneity, i.e., the presence of inactive monomers or irreversible polymers (Squire & Li, 1961). All experiments were done in 20 mM Hepes, 5 mM MgAcetate, 0.1 mM EDTA, 0.1 mM EDTA, 50 mM KAcetate, 0.1 mM DTT, and 30 μM ATP, pH 7.2, unless otherwise noted. The density of the buffer was determined in a Mettler-Parr DMA 02D precision density meter to be 1.0014 gm/mL at 24.6 °C. Buffer viscosity (0.9296 at 24.6 °C) was measured in a Cannon–Manning semimicro viscometer. The partial specific volume of each construct was calculated by the method of Cohen and Edsall and included the effect of a single bound nucleotide molecule (Laue et al., 1992; $\bar{\nu}_{K401} = 0.7339$, $\bar{\nu}_{K366} = 0.7336$; $\bar{\nu}_{K341} = 0.7336$). The inclusion of nucleotide in this calculation decreased $\bar{\nu}$ by 0.0030. Because the temperature was calibrated and the buffer density and viscosity were measured, the single largest source of error in these molecular weight measurements is the $\bar{\nu}$ estimation. If we use the values of Zamyatnin (1972 or 1984) rather than the Cohen and Edsall values, the molecular weight estimates are decreased by approximately 4.3% and 7.1%, respectively. It is generally accepted that the Cohen and Edsall values give the most reliable molecular weights (Perkins, 1986), and this method appears to be confirmed by the study presented here (see Discussion).

RESULTS

Sedimentation Velocity Studies of K401. Figure 1 presents corrected sedimentation coefficients for K401 plotted as a function of K401 concentration. The sedimentation coefficient increases with increasing K401 concentration, and identical results were obtained in the presence of either added 30 μM ADP (□) or added 30 μM AMPPNP (△). The extrapolated sedimentation coefficient is 5.06 S. Representative sedimentation coefficient distributions for K401 are presented in Figure 2. The sedimentation coefficient distributions are nearly symmetric and clearly shift to a higher S value with increasing K401 concentration. Fits with SVEDBERG in general were best described by single species, with a second species between 10 and 12.5 S never exceeding 4.4% of the total material. Nearly half of the two species fits failed to converge, indicating the absence of heterogeneity or a second boundary. As described in Experimental Procedures, the values plotted in Figure 1 are derived from SVEDBERG and agree with the analysis by migration of the maximum gradient, dc/dr, position, and the peak position of the $g(s)$ analysis. To establish the molecular weight of the 5.06-S species and the nature of the concentration-dependent self-association, sedimentation equilibrium experiments were conducted.

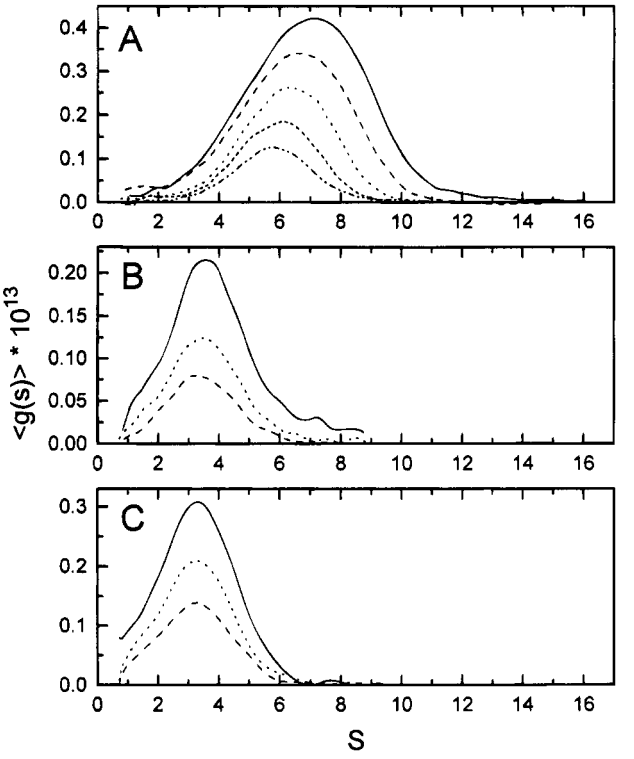

FIGURE 2: Sedimentation coefficient distribution analysis. The sedimentation velocity data were analyzed for the sedimentation distribution, $g(s)$, as described Experimental Procedures. Panel A presents data for K401 in the presence of 30 μM ATP at 3.6, 5.4, 8.7, 12.7, and 18.1 μM, corresponding to the lowest to the highest peak in the figure. Panel B presents data for K366 at 1.6, 2.4, and 4.3 μM. Panel C presents data for K341 at 2.4, 3.6, and 6.0 μM.

Sedimentation Equilibrium Studies with K401. Equilibrium experiments were conducted on initial concentrations[2] of K401 between 0.5 and 3.0 μM at 16 000 (Figure 3) and 20 000 rpm (Figure 4). All channels can be fit by a model of 1–2–4 (monomer–dimer–tetramer), or equally well by a model of 1–2–3 (monomer–dimer–trimer). The results

[2] There appeared to be a dramatic nonlinearity of the signal at the low concentrations. Note that the data set at 0.5 μM loading concentration has very little curvature (Figure 4A). Data sets at 0.1 and 0.25 μM loading concentration had little or no curvature and could not be analyzed. We ascribe this apparent loss of signal to adsorption of K401 to the windows and walls of the centerpiece.

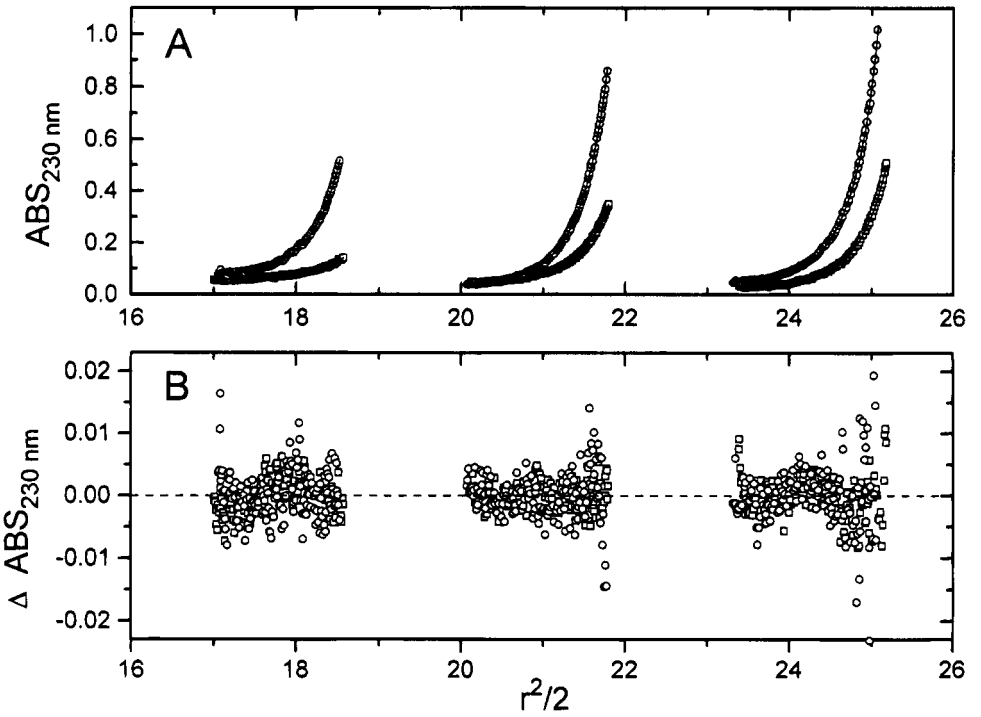

FIGURE 3: Sedimentation equilibrium data for K401 at 16 000 rpm, 25 °C. Initial concentrations were 0.5, 0.75, 1.0, 1.5, 2.0, and 3.0 μM K401. Panel A presents the data sets and the results of a global fit of all six data sets to a monomer−dimer−tetramer model. Data sets were truncated to 1.0 OD to improve the randomness of the fit. The resulting equilibrium constants are summarized in Table 1. Panel B presents a composite residual plot for the global fit in panel A.

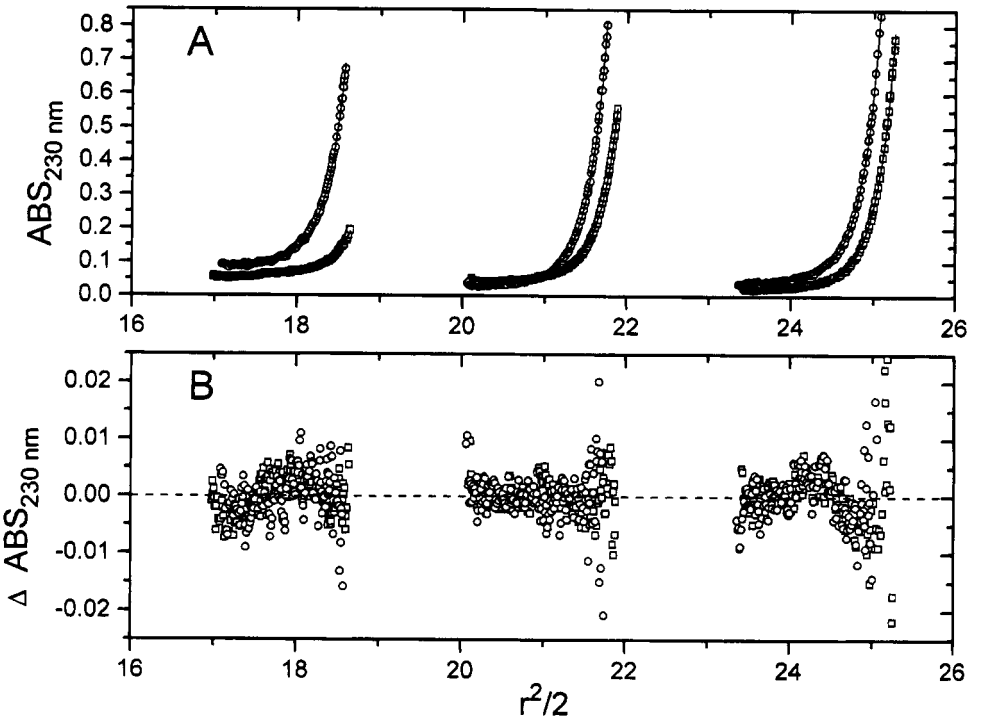

FIGURE 4: Sedimentation equilibrium data for K401 at 20 000 rpm, 25 °C. Initial concentrations were 0.5, 0.75, 1.0, 1.5, 2.0, and 3.0 μM K401. Panel A presents the data sets and the results of a global fit of all six data sets to a monomer−dimer−tetramer model. Data sets were truncated to 0.8 OD to improve the randomness of the fit. The resulting equilibrium constant are summarized in Table 1. Panel B presents a composite residual plot for the global fit in panel A.

of the 1−2−4 model are presented in Table 1. (Note: K_4 corresponds to the overall formation of tetramer from four monomers, regardless of the pathway to assembly, i.e., dimerization of dimers or successive addition of monomers.) Experiments were also conducted in the presence of ADP and AMPPNP at 16 000 rpm. The ADP and AMPPNP data are best fit by a model involving 1−2−4 or 1−2−4−8 (Figure 5), although the 1−2−4−8 fits are only marginally better (i.e., rms of 4.04 and 3.41 × 10^{-3} vs 4.06 and 3.48 × 10^{-3} for the 1−2−4 fits). A repeat of the ATP conditions at the same time are still best fit by a 1−2−4 or a 1−2−3 model. Attempts to fit the ATP data to a 1−2−4−8 model were successful, but the rms values of the fits are not improved, the error on K_8 was extremely large, and the values of K_2 and K_4 are unchanged. The 1−2−4 model is preferred over the 1−2−3 model for ATP−K401 because the best

Table 1: Sedimentation Equilibrium Results with K401 + ATP

speed	K_2 (M^{-1})	K_4 (M^{-3})	rms[a] ($\times 10^{-3}$)
16K[b]	4.54×10^7	2.55×10^{20}	3.52
	$\langle 2.69 \times 10^7, 9.03 \times 10^7 \rangle$[c]	$\langle 1.08 \times 10^{20}, 7.95 \times 10^{20} \rangle$	
20K	4.04×10^7	1.13×10^{20}	4.11
	$\langle 2.45 \times 10^7, 7.96 \times 10^7 \rangle$	$\langle 5.76 \times 10^{19}, 2.83 \times 10^{20} \rangle$	
16K[d]	1.34×10^8	2.10×10^{21}	4.49
	$\langle 4.90 \times 10^7, 4.37 \times 10^8 \rangle$	$\langle 3.19 \times 10^{20}, 1.91 \times 10^{22} \rangle$	
	Global Fit of all ATP Data		
16 & 20K	2.74×10^7	9.43×10^{19}	4.23
	$\langle 1.78 \times 10^7, 4.82 \times 10^8 \rangle$	$\langle 4.83 \times 10^{19}, 2.27 \times 10^{20} \rangle$	

[a] Root mean square deviation of the fit in OD units. [b] First experiment at 16K as shown in Figure 3. [c] Corresponds to a 95% confidence interval or ±2 SD.

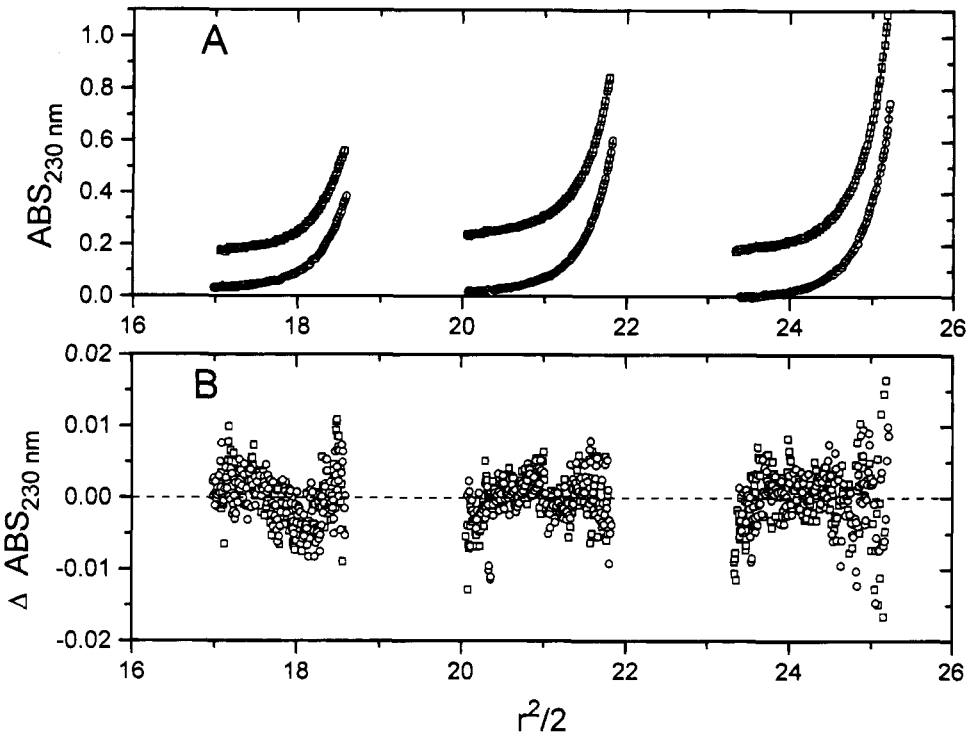

FIGURE 5: Sedimentation equilibrium data on K401 at 16 000 rpm, 25 °C, in the presence of (□) 30 μM ADP or (○) 30 μM AMPPNP. Initial concentrations were 1.0, 1.5, and 2.0 μM K401. The ADP data sets are offset by 0.2 for clarity. The data sets required no truncation to improve the randomness of the residuals, and the three data sets in each case were globally fit to a 1−2−4−8 model. A 1−2−4 model is statistically equivalent. Equilibrium constants for the 1−2−4 fit are presented in Table 2. Panel B is a composite residual plot for the fits presented in panel A. (□) 30 μM ADP; (○) 30 μM AMPPNP.

Table 2: K401 Sedimentation Equilibrium Results with AMPPNP and ADP

speed	K_2 (M^{-1})	K_4 (M^{-3})	rms[a] ($\times 10^{-3}$)
	AMPPNP		
16K	2.39×10^7	1.44×10^{20}	3.48
	$\langle 1.28 \times 10^7, 4.66 \times 10^7 \rangle$[b]	$\langle 4.99 \times 10^{19}, 4.48 \times 10^{20} \rangle$	
	ADP		
16K	2.85×10^7	1.18×10^{20}	4.06
	$\langle 1.45 \times 10^7, 6.01 \times 10^7 \rangle$	$\langle 3.75 \times 10^{19}, 4.23 \times 10^{20} \rangle$	
	Global Fit of all 16K Data: ATP, ADP, and AMPPNP		
16K	6.04×10^7	4.82×10^{20}	4.01
	$\langle 3.32 \times 10^7, 1.22 \times 10^8 \rangle$	$\langle 1.69 \times 10^{20}, 1.67 \times 10^{21} \rangle$	

[a] Root mean square deviation of the fit in OD units. [b] Corresponds to a 95% confidence interval or ±2 SD.

fitted value of K_2 is identical for both the 16K and the 20K data and is furthermore identical within error to the value of K_2 in the 1−2−4 fits of the ADP or AMPPNP data. For 1−2−3 fits, the value of K_2 is speed dependent. A summary of the fitted equilibrium constants are presented in Tables 1 and 2. A joint 1−2−4 fit of all the ATP-K401 data, corresponding to 15 channels and 2400 data points, gives a K_2 value corresponding to a K_d for dimer dissociation of 37 nM with a 95% confidence interval of ⟨56 nM, 21 mM⟩ (Table 1; Johnson et al., 1981).

For the ADP and AMPPNP data sets the K_d values for dimer dissociation are 35 ± 26 and 42 ± 28 nM, respectively. The 1−2−4−8 fits of the ADP and AMPPNP data sets give even lower estimates of K_d, 13 and 3 nM, respectively, but these values are probably suspect due to correlated error propagation in the nearly overdetermined fit

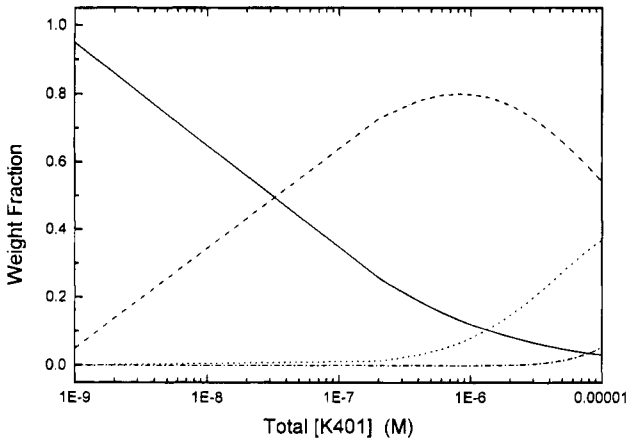

FIGURE 6: Species plot of the weight fraction of monomer−dimer−tetramer−octamer concentrations over the total K401 concentration range of 1 nM to 10 μM. Symbols are (−) monomer, (− −) dimer, (• • •) tetramer, and (− • −) octamer. The simulation was done with the parameters from the joint fit of Table 1, $K_2 = 2.74 \times 10^7$ M^{-1}, and $K_4 = 9.43 \times 10^{19}$ M^{-3}, with addition of the maximal value of K_8 found for the ADP and AMPPNP data sets, 7.02×10^{44} M^{-7}. Note that the dimer species is predominant above the K_d, 37 nM, and remains so through the entire concentrations range shown, peaking at approximately 1 μM.

(Johnson & Frasier, 1985). It is for this reason that only parameters from a 1−2−4 fit are compared directly in Tables 1 and 2. A global fit of all the 16K data sets (ATP, ADP, AMPPNP) to a 1−2−4 model gave a global estimate of the K_d for dimer dissociation of 17 nM with a 95% confidence interval of ⟨30 nM, 8 nM⟩ (Table 2; Johnson et al., 1981). All of the residuals for the different data sets were reasonably random, consistent with a similar mechanism of assembly in the presence of ATP, ADP, and AMPPNP. A species distribution plot, based upon this global fit, is presented in Figure 6 over the range of 1 nM to 10 μM K401. The weight fraction of dimer becomes predominant above the K_d for dimer dissociation and peaks near 1 μM total K401. Above 1 μM total K401 tetramer becomes significant but does not exceed the weight fraction of dimer. The weight fraction of octamer is not significant below 10 μM total K401, and since we have used an upper estimates of K_8 in this simulation, we conclude that octamer is a minor component in these solutions and can in general be ignored.

On the basis of the results of the sedimentation equilibrium data and the simulation presented in Figure 6, we conclude that the concentration-dependent increase in the $s_{20,w}$ of K401 (Figure 1) corresponds to a dimer−tetramer equilibrium. Note that an interacting boundary involving pseudodimerization (i.e., dimer to tetramer) is not expected to resolve into multiple zones, but will reflect the weight average concentration of dimer and tetramer, as has been documented for interacting systems obeying Gilbert theory (Gilbert, 1959; Na & Timasheff, 1985). At higher concentrations octamer is evident but only in small amounts.

Sedimentation Velocity Studies with K366. Figure 1 presents corrected sedimentation coefficients for K366 (*) plotted as a function of K366 concentration. A linear fit of the data gives $s^0_{20,w} = 3.25$ S. Figure 2B presents the sedimentation coefficient distribution, $g(s)$, for solutions of K366. The distributions are reasonably symmetric with some indication of higher molecular weight forms. Fits with SVEDBERG required two species for all three data sets, with the major component corresponding to the 3.25-S species and a minor component near 8−9 S. The minor component

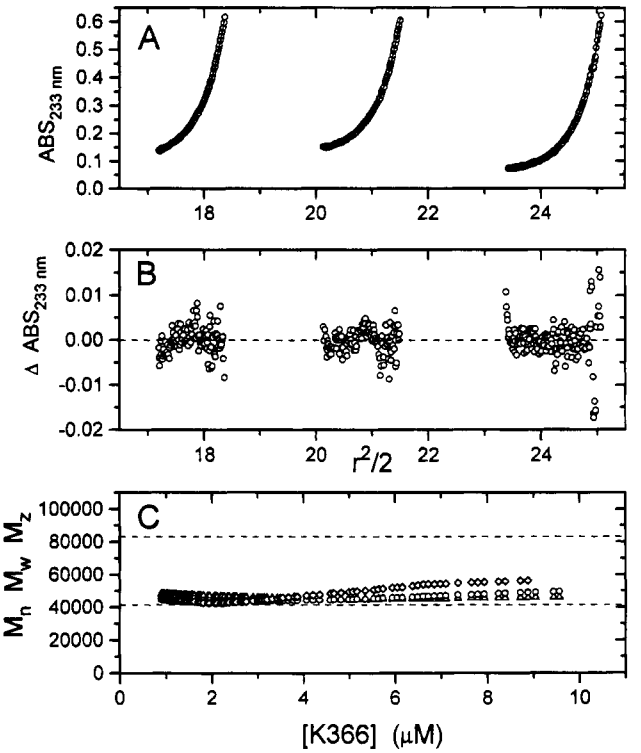

FIGURE 7: Sedimentation equilibrium data on K366 at 22 000 rpm, 25 °C. Initial concentrations were 6.8, 5.2, and 3.7 μM K366 for channels A−C. Panel A presents a data truncated to 0.6 OD_{233} and the global fit of the three channels to a single ideal species. Panel B presents the corresponding residuals. Panel C presents Biospin analysis of the data set at an initial concentration of 5.2 μM K366. The symbols represent M_n (△), M_w (○), and M_z (◇), respectively. These data are consistent with homogeneity below 4 μM K366, corresponding to the region where data were truncated to achieve a good single-species fit. The untruncated data sets could be fit to a 1−2−8 or a 1−2−4−8 model, although small systematic deviations remained (data not shown).

Table 3: Fitting of K366 Equilibrium Data with NONLIN

channel	M_z	⟨−, +⟩[a]	rms[b] ($\times 10^{-3}$)
A	40 574	⟨39 346, 41 913⟩	2.32
B	41 429	⟨40 135, 42 818⟩	2.32
C	42 469	⟨40 570, 44 432⟩	4.28
joint	41 768	⟨40 585, 43 022⟩	3.20

[a] Corresponds to a 95% confidence interval or ±2 SD. [b] Root mean square deviation of the fit in OD units.

represented 2%, 6.8%, and 8.3% of the total material with increasing loading concentration. Three species fits failed to converge; however, this does exclude a distribution of larger aggregates. Sedimentation equilibrium experiments were conducted to determine the size of the 3.25-S species and the nature of the larger aggregates.

Sedimentation Equilibrium Studies with K366. Figure 7 presents the fitting of K366 equilibrium data to a single-component model. The results of the fits are summarized in Table 3. Joint fitting of all three channels gives a molecular weight within 0.9% of the K366 monomer species, and the fits of the individual channels are within ±2.5% of the expected molecular weight. To achieve random residuals, the data had to be truncated to <0.6 OD_{233} (Figure 7A,B). Higher molecular weight forms are present, but a monomer−dimer model does not fit the data. However, the data set up to 1.0 OD can be fit reasonably well by a model including 1−2−8 or 1−2−4−8 with octamer the favored polymer species. This is consistent with a small amount of 8−9 S

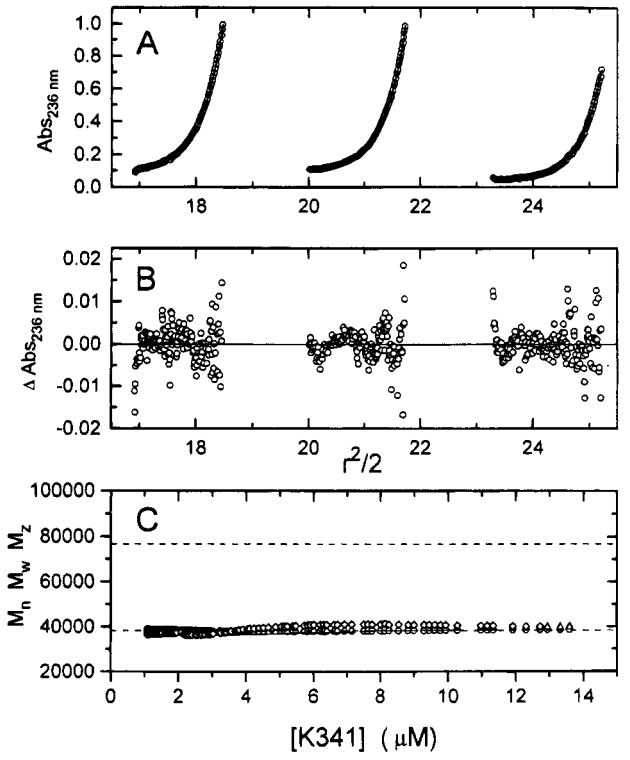

FIGURE 8: Sedimentations equilibrium data on K341 at 24 000 rpm, 25 °C. Loading concentrations were 6.9, 5.1, and 2.8 μM K341 for channels A−C. Panel A: The data and a global fit of the three channels to a single-component model. All data sets were truncated at 1.0 OD to avoid nonlinear absorbance effects and to improve the fits. The resulting molecular weights are presented in Table 4. Panel B is a residual plot of the difference between the fit and the data. Panel C presents Biospin analysis of the data set at an initial concentration of 6.9 μM K341. The symbols represent M_n (△), M_w (○), and M_z (◇), respectively. These data are consistent with a single homogeneous species in solutions of K341.

component in the velocity data. The analysis of these data with Biospin is also consistent with a small fraction of higher molecular weight forms being present above 4−5 μM K366 (Figure 7C).

Sedimentation Velocity Studies with K341. Figure 1 presents corrected sedimentation coefficients for K341 (●) plotted as a function of K341 concentration. A linear fit to the data gives an $s^0_{20,w}$ = 2.9 S. Figure 2C presents the sedimentation coefficient distributions, $g(s)$, for solutions of K341. The distributions are very symmetric, suggesting a single species in solution. Analyses of the two lower concentration runs with SVEDBERG are also consistent with a single species in solution. However, the velocity runs at 6 μM are consistent with a small amount of larger species (between 10.3 and 13.8%) at 4.1−4.5 S. If this second species were a dimer, this would correspond to a K_d between 47 and 33 μM. To determine the size of the major species in solution, sedimentation equilibrium experiments were performed.

Sedimentation Equilibrium Studies with K341. Figure 8 presents the fitting of K341 equilibrium data to a single-component model. The results of the fits are summarized in Table 4. The joint fitting of all three channels gives a molecular weight within 0.2% of the expected sequence molecular weight, and the fits of the individual channels are within ±2.5% of the expected molecular weight. An absorbance of 1.0 at 236 nm corresponds to approximately 10 μM K341. Thus we conclude that K341 is a monomer at concentrations below 10 μM. At higher concentrations

Table 4: Fitting of K341 Equilibrium Data with NONLIN

channel	M_z	⟨−, +⟩[a]	rms[b] (×10^{-3})
A	37 399	⟨36 475, 38 337⟩	3.95
B	38 242	⟨37 457, 39 023⟩	3.52
C	39 263	⟨38 192, 40 334⟩	3.87
joint	38 191	⟨37 458, 38 925⟩	4.08

[a] Corresponds to a 95% confidence interval or ±2 SD. [b] Root mean square deviation of the fit in OD units.

the fits to a single species are systematic, suggesting larger species in solution, probably corresponding to the additional species evident in the 6 μM velocity runs.[3] The data are not consistent with these larger species being exclusively dimer. A monomer−dimer model does not significantly improve the rms values of the fits, while the K_d of the fit is extremely large, 14.3 mM. Fits to more complex models, i.e., 1−2−4, failed to converge. Analysis of these data sets with Biospin are also consistent with a single species in solution, as is evident by the superposition of the number-, weight-, and Z-average molecular weight (Figure 8C). Thus, the equilibrium data are consistent with K341 existing as a monomer. Deviations in the residuals for data points above 1.0 OD_{236} are consistent with a small amount, <10%, of irreversible aggregation at higher protein concentrations.[3]

DISCUSSION

The sedimentation velocity and sedimentation equilibrium results described here are consistent with kinesin construct K401 undergoing a 1−2−4 mechanism of self-association, i.e., involving dimerization and the subsequent dimerization of dimers. The dissociation constant for the dimer formation corresponds to 37 nM in the presence of ATP and is independent of the nucleotide bound, being 35 nM with ADP and 42 nM with AMPPNP. We assume that the 30 μM ATP added to the kinesin preparations was converted to ADP prior to the reaction reaching equilibrium during the centrifuge run. With a k_{cat} of ca. 0.01 s^{-1} in the absence of microtubules for K401, K366, and K341, the 30 μM ATP would be hydrolyzed to ADP to ~30 min. Identical results with the nonhydrolyzable ATP analog AMPPNP support the conclusion that K401 self-association, in the absence of microtubules, is independent of the nucleotide bound, ADP or ATP. This conclusion requires that nucleotide binding be a high-affinity process, i.e., $K_d \ll 30$ μM, although this is currently not known. However, in the absence of added nucleotide, K401 is prone to extensive irreversible aggregation during a sedimentation equilibrium run (data not shown). Identical reversible association events in the ATP, ADP, and AMPPNP solutions (Tables 1 and 2) is evidence for tight binding of these nucleotides to K401.

The rather small K_d for K401 dimer dissociation has important implications for the interpretation of motility studies in the nanomolar concentration range. Below 37 nM K401, the construct will be predominantly monomeric (Figure 6). We have shown that both K366 and K341 are monomeric below 4 and 10 μM, respectively, and further-

[3] A second potential source of deviation at high absorbance gradient values is Weiner skewing, caused by a poor alignment of the light source focal plane (Svensson, 1954). Alignment above the 2/3 position of the centerpiece will cause deviations resembling aggregation; alignment below the 2/3 position of the centerpiece will cause deviations resembling nonideality. Alignment of the monochromator is factory set and cannot be adjusted by the user.

more appear to display ATPase abilities that are somewhat uncoupled from motility along microtubules (Stewart et al., 1993; M. L. Moyer, S. P. Gilbert, and K. A. Johnson, manuscript in preparation). Similar behavior may occur at dilute concentrations of K401. Alternatively, either monomeric K401 may have reduced affinity for the microtubule lattice, and thus reduced activity, or binding of dimers may be a cooperative process, similar to many DNA binding proteins (Steitz, 1993; Austin, et al., 1994), and thus the effective K_d may be reduced in the presence of microtubules by a coupled binding event. The mechanistic studies published by Gilbert and Johnson (Gilbert & Johnson, 1993, 1994; Gilbert et al., 1995) used microtubule−K401 complexes that were performed at K401 concentrations >1 μM followed by dilution to the desired concentration. These studies and the results presented here suggest that the microtubules may stabilize the dimeric state of K401 at lower protein concentrations. However, it is apparent that to interpret experiments at low kinesin concentrations requires that the monomer, dimer, and higher oligomer equilibrium be considered.

At higher concentrations of K401 tetramers and possibly octamers will form. During the course of these studies we analyzed one preparation of K401 purified in the absence of nucleotide. This preparation was less active and lacked the ability to reversibly associate, although it was >60% dimer and formed extensive irreversible polymers (data not shown). Thus, kinesin motor domain K401 appears to be prone to irreversible aggregation in concert with decreased activity, while active K401 is capable of undergoing reversible self-association. It is not clear whether these reversible polymers bind to microtubules or display motility activity. A cooperative process or steric hindrance could again favor the exclusive binding of dimers, but this is not known. [Note for example that λ cI repressor dimers are believed to cooperatively associate into tetramers at adjacent sites on DNA but have recently been shown to form a concerted octomer in solution (Senear et al., 1993)]. EM studies have been interpreted in terms of kinesin dimers decorating the microtubule lattice. However, the difference between a dimer and a tetramer may not be obvious, especially if one is not looking for it. K401 is reported to bind to microtubules at a ratio of one motor domain to one tubulin heterodimer with a preference for β-tubulin (Harrison et al., 1993; Song et al., 1993). At ratios of K401 to tubulin exceeding 2:1 the binding of higher polymers has not been reported, but these higher order oligomers may not be detectable. The mechanism of assembly that best fits the self-association data for K401 is 1−2−4. This mechanism suggests the additional possibility that native kinesin may undergo higher order association as well, either by interactions at the head domain or by stalk−stalk interaction, similar to the self-association of myosin (Godfrey & Harrington, 1970a,b). In fact, Berliner et al. (1994) have reported preliminary sedimentation and EM studies on construct K612-BIO that suggest a tetramer structure mediated by the stalk. Future studies on larger motor domain constructs and intact kinesin dimers will test this possibility.

The loss of the ability to form dimers with high affinity demonstrated by constructs K366 and K341 suggests that the sequence of amino acids located between positions 367 and 401 are directly or indirectly involved in the formation of a dimer interface. High-resolution structural information is required to ascertain a molecular explanation of this lost activity. The presence of low concentrations of octamer in the K366 samples, as evidenced by an 8−9-S boundary in the velocity data and a best fit of the higher concentration equilibrium data to a 1−2−8 model, suggest that higher oligomer formation is mediated by other regions of the protein. We cannot exclude the possibility that octamers of K366 form by a nonspecific mechanism unrelated to octamer formation of K401, but the utilization of similar contacts is the simplest assumption to make at this time. Aggregates of K341 appear to be unrelated to the weak self-association displayed by K366 or the strong self-association displayed by K401. It seems safe to speculate that the self-association domains responsible for dimerization and the additional 2−4−8 assembly have been removed or seriously hindered in the K341 construct. Furthermore note that, except for nucleotides, we have not systematically investigated the role of other effectors of self-association, i.e., Mg^{2+}, temperature, pH, ionic strength, etc., and we cannot exclude the possibility of changes in the extent of mechanism of self-association displayed by these constructs under other solution conditions. Other studies performed in the presence of sucrose are in complete agreement with the qualitative conclusion that K401 is predominantly a dimer and smaller constructs like K341 are predominantly monomers (Huang et al., 1994), although caution in the use of osmolytes for these studies has been noted (Cann et al., 1994). These sucrose density velocity studies could not, however, determine the K_d for dimer dissociation or the presence of higher order polymers.

The sedimentation coefficient of a macromolecule is dependent upon the molecular weight and the frictional coefficient or shape of the particle. To interpret sedimentation velocity data in terms in shape information, we must first estimate the degree of hydration expected for these peptides. Using the hydration data of Kuntz (Kuntz, 1971; Lee & Timasheff, 1979) appropriate for pH 6.0−8.0, we calculate the degrees of hydration to be 0.43, 0.43, and 0.41 gm/gm, respectively, for K401 K366, and K341. These are likely to be overestimates due to solvent-inaccessible regions, but we will assume 0.4 gm/gm of bound water for all subsequent calculations. The sedimentation velocity boundary with K401 is a reversibly interacting system of predominantly dimer−tetramer (Figures 1 and 6). Thus, the extrapolated $s_{20,w}$ value of 5.06 may be slightly large for a dimer. However at ca. 1 μM K401 the solution should be 80% dimer (Figure 6), and thus assigning the dimer an $s^0_{20,w}$ value of 5.06 S will be approximately correct. An $s_{20,w}$ of 5.06 is rather small for a 91 064 molecular weight molecule (dimer−ADP complex) and is consistent with a Stokes radius of 34.5 Å, an f/f_0 = 1.21, and an axial ratio for a prolate ellipsoid of 7.82. An elongated shape for a K401 dimer may have significance for its interaction with microtubules. The $s^0_{20,w}$ value for K366 is equally small for a 41 404 molecular weight molecule (monomer−ADP complex) and is consistent with a Stokes radius of 26.5 Å, an f/f_0 = 1.12, and an axial ratio for a prolate ellipsoid of 4.72. Finally, the $s^0_{20,w}$ value for K341, a 38 274 molecular weight molecule (monomer−ADP complex), is consistent with a Stokes radius of 25.8 Å, an f/f_0 = 1.19, and an axial ratio for a prolate ellipsoid of 7.07. While errors in other parameters may be partial explanations for the deviation from spherical behavior, the data for all three constructs suggest irregularly shaped monomers and dimers.

The affinity constants for dimerization summarized in Tables 1 and 2 correspond to a total free energy of interaction

between the two heads of -10.45 ± 0.36 kcal/mol. This is evidence that our estimates of the dimerization constants are highly precise and a strong indication that the dimerization of K401 is not dependent upon the type of nucleotide bound. The accuracy or absolute value of the affinity is dependent upon the extinction coefficients used. However, even a value that attempts to correct for the contribution of bound ADP, i.e., $26740 \pm 2500\ M^{-1}$ for K401 (Gilbert & Johnson, 1993), will only increase the free energy of interaction by -0.05 kcal/mol, an amount less than the uncertainty of the free energy estimate. The major source of uncertainty actually resides in the reduced molecular weight, σ_1, used in the association scheme. Small changes in σ_1 due to uncertainty in $\bar{\nu}$ will cause shifts in the fitted K_2 and K_4 values. For example, using the data of Zamyatnin (1972) rather than the Cohen and Edsall data set to estimate $\bar{\nu}$ and reanalyze the first 16K ATP data set will decrease K_2 by a factor of 2.0 and ΔG^0 by 0.42 kcal/mol. Fortunately, K366 and K341 are monomeric and of known molecular weight. Since our best estimates of the Z-average molecular weight for K366 and K341 are within 0.9% and 0.2%, respectively, of the appropriate nucleotide−complex molecular weight, we have confidence that our estimates of σ_1 for K401 are also likely to be correct, and thus that our estimates of K_2 and K_4 are accurate. (An additional caveat is that there are no volume changes upon self-association of K401 that affect the $\bar{\nu}$ of the polymers. Only pressure-dependent studies could resolve this concern.) Finally, note that the ΔG^0/K401 monomer added for dimerization is -10.45 ± 0.36 kcal/mol, while the ΔG^0/K401 monomer added for tetramer formation is -9.30 ± 0.36 kcal/mol. This accounts for the predominance of K401 dimers over tetramers in solution.

In conclusion, the sedimentation studies reported here establish the mode of self-association of the kinesin motor domain construct K401 to be 1−2−4. Between ca. 37 nM and 10 μM total K401, dimer is the prevalent species. This association behavior is independent of the nucleotide bound, i.e., ADP or AMPPNP and thus by inference ATP. Removal of additional amino acids from the motor domain to generate smaller constructs dramatically reduces self-association such that only monomeric species are present up to 4 μM K366 and 10 μM K341, respectively. This suggests that the amino acids located between positions 367 and 401 are directly or indirectly involved in the formation of a dimer interface. This observation appears to explain the altered uncoupling of ATP hydrolysis and force production for K366 and K341, and it strongly suggests that dimer formation is required for the distinctive processive motility behavior of kinesin. In addition, the kinetics revealed that the motor domains of the dimer release sequentially from the microtubule, therefore increasing the time during the cycle when kinesin is bound to the microtubule (Gilbert et al., 1995). These kinetic results have provided a mechanistic model to account for the apparent processive motility. K401 behaves kinetically as a processive enzyme in single-turnover experiments (Gilbert et al., 1995). K366 and K341 show elevated steady-state ATPase activity (k_{cat} = 70 and 95 s^{-1}, respectively) in comparison to K401 (k_{cat} = 20 s^{-1}) and promote motility at rates less than the rates of translocation produced by the longer kinesin polypeptides (Stewart et al., 1993). These results suggest that, for the shorter constructs, ATP hydrolysis and force production are partially uncoupled. Furthermore, the data indicate that there are cooperative interactions between the kinesin motor domains that are required to produce the processive behavior observed kinetically and in the motility experiments. However, this hypothesis of cooperativity between the head domains must be tested rigorously. In larger constructs like K401 the role of a monomer−dimer−tetramer reaction in force production is unclear, and future studies will need to consider this equilibrium in the interpretation of motility data.

ACKNOWLEDGMENTS

We thank Alex Slawson for assistance with the temperature calibration of the XLA. We thank the National Analytical Ultracentrifuge Center, Storrs, CT; Emory Braswell; Jeff Lary; Walter Stafford; John Philo; and Amgen, Inc.; for providing software used in this analysis.

REFERENCES

Allen, R. D., Weiss, D. G., Hayden, J. H.; Brown, D. T., Fujiwake, H., & Simpson, M. (1985) *J. Cell Biol. 100*, 1736−1752.
Austin, D. J., Crabtree, G. R., & Schrieber, S. L. (1994) *Chem. Biol. 1*, 131−136.
Berliner, E., Mahtani, H. K., Karki, S., Chu, L. F., Cronan, J. E., Jr., & Gelles, J. (1994) *J. Biol. Chem. 269*, 8610−8615.
Berliner, E., Young, E. C., Anderson, K., Mahtani, H. K., & Gelles, J. (1995) *Nature 373*, 718−721.
Block, S. M., Goldstein, L. S. B., & Schnapp, B. J. (1990) *Nature 348*, 348−352.
Bradford, M. M. (1976) *Anal. Biochem. 72*, 248−254.
Cann, J. R., Coombs, R. O., Howlett, G. J., Jacobson, M. P., & Winzor, D. J. (1994) *Biochemistry 33*, 10185−10190.
Cohn, S. A., Ingold, A. L., & Scholey, J. M. (1989) *J. Biol. Chem. 264*, 4290−4297.
de Cuevas, M., Tao, T., & Goldstein, L. S. (1992) *J. Cell Biol. 116*, 957−965.
Gelles, J., Schnapp, B. J., & Sheetz, M. P. (1988) *Nature (London) 331*, 450−453.
Gho, M., McDonald, K., Ganetzky, B., & Saxton, W. M. (1992) *Science 258*, 313−316.
Gilbert, G. A. (1959) *Proc. R. Soc. London, Ser. A 250*, 377−388.
Gilbert, S. P., & Johnson, K. A. (1993) *Biochemistry 32*, 4677−4684.
Gilbert, S. P., & Johnson, K. A. (1994) *Biochemistry 33*, 1951−1960.
Gilbert, S. P., Webb, M. R., Brune, M., & Johnson, K. A. (1995) *Nature 373*, 671−676.
Gill, S. C., & von Hippel, P. H. (1989) *Anal. Biochem. 182*, 319−326.
Godfrey, J. E., & Harrington, W. F. (1970a) *Biochemistry 9*, 887−893.
Godfrey, J. E., & Harrington, W. F. (1970b) *Biochemistry 9*, 894−908.
Harrison, B. C., Marchese-Ragona, S. P., Gilbert, S. P., Cheng, N., Steven, A. C., & Johnson, K. A. (1993) *Nature 362*, 73−75.
Hirokawa, N., Pfister, K. K., Yorifuji, H., Wagner, M. C., Brady, S. T., & Bloom, G. S. (1989) *Cell 56*, 867−878.
Howard, J., Hudspeth, A. J., & Vale, R. D. (1989) *Nature 342*, 154−158.
Huang, T. G., & Hackney, D. D. (1994) *J. Biol. Chem. 269*, 16493−16501.
Huang, T. G., Suhan, J., & Hackney, D. D. (1994) *J. Biol. Chem. 269*, 16502−16507.
Hunt, A. J., Gittes, F., & Howard, J. (1994) *Biophys. J. 67*, 766−781.
Johnson, M. L., & Frasier, S. G. (1985) *Methods Enzymol. 117*, 301−341.
Johnson, M. L., Correia, J. J., Yphantis, D. A., & Halvorson, H. R. (1981) *Biophys. J. 36*, 575−588.
Kuo, S. C., & Sheetz, M. P. (1993) *Science 260*, 232−234.
Kuntz, I. D. (1971) *J. Am. Chem. Soc. 93*, 514−516.
Lansing, W. D., & Kraemer, E. O. (1935) *J. Am. Chem. Soc. 57*, 1369−1377.
Lasek, R. J., & Brady, S. T. (1985) *Nature 316*, 645−647.
Laue, T. M., Shah, B. D., Ridgeway, T. M., & Pelletier, S. L. (1992) in *Analytical Ultracentrifugation in Biochemistry and Polymer*

Science (Harding, S. E., Rowe, A. J., & Horton, J. C., Eds.) pp 90−125, Royal Society of Chemistry, Cambridge.
Lee, J. C., & Timasheff, S. N. (1979) *Methods Enzymol. 61*, 49−62.
Liu, S., & Stafford, W. F., III (1995) *Anal. Biochem. 224*, 199−202.
Na, G. C., & Timasheff, S. N. (1985) *Methods Enzymol. 117*, 459−495.
Philo, J. (1994) in *Modern Analytical Ultracentrifugation: Acquisition and Interpretation of Data for Biological and Synthetic Polymer Systems* (Schuster, T. M., & Laue, T. M., Eds.) pp 156−170, Birkhauser Boston, Inc., Cambridge, MA.
Perkins, S. J. (1986) *Eur. J. Biochem. 157*, 169−180.
Porter, M. E., Scholey, J. M., Stemple, D. L., Vigers, G. P., Vale, R. D., & Sheetz, M. P. M., Jr. (1987) *J. Biol. Chem. 262*, 2794−2802.
Ray, S., Meyhofer, E., Milligan, R. A., & Howard, J. (1993) *J. Cell Biol. 121*, 1083−1093.
Roark, D. E., & Yphantis, D. A. (1968) *Ann. N.Y. Acad. Sci. 164*, 245−278.
Romberg, L., & Vale, R. D. (1993) *Nature 361*, 168−170.
Rosenberg, A. H., Lade, B. N., Chui, D., Lin, S., Dunn, J. J., & Studier, F. W. (1987) *Gene 56*, 125−135.
Senear, D. F., Laue, T. M., Ross, J. B. A., Waxman, E., Eaton, S., & Rusinova, E. (1993) *Biochemistry 32*, 6179−6189.
Song, Y.-H., & Mandelkow, E. (1993) *Proc. Natl. Acad. Sci. U.S.A. 90*, 1671−1675.
Squire, P. G., & Li, C. H. (1961) *J. Am. Chem. Soc. 83*, 3521−3528.
Stafford, W. F., III (1992a) *Anal. Biochem. 203*, 295−301.
Stafford, W. F., III (1992b) in *Analytical Ultracentrifugation in Biochemistry and Polymer Science* (Harding, S. E., Rowe, A. J., & Horton, J. C., Eds.) pp 359−393, Royal Society of Chemistry, Cambridge.
Steitz, T. A. (1993) *Structural Studies of Protein-Nucleic Acid Interaction*, Cambridge University *Press*, Cambridge.
Stewart, R. J., Thaler, J. P., & Goldstein, L. S. (1993) *Proc. Natl. Acad. Sci. U.S.A. 90*, 5209−5213.
Studier, R. W., Rosenberg, A. H., Dunn, J. J., & Dubendorff, J. W. (1990) *Methods Enzymol. 185*, 60−89.
Svensson, H. (1954) *Opt. Acta 1*, 25−32.
Svoboda, K., & Block, S. M. (1994) *Cell 77*, 773−784.
Svoboda, K., Schmidt, C. F., Schnapp, B. J., & Block, S. M. (1993) *Nature 365*, 721−727.
Uyeda, T. Q. P., Warrick, H. M.; Kron, S. J., & Spudich, J. A. (1991) *Nature 352*, 307−311.
Vale, R. D., Reese, T. S., & Sheetz, M. P. (1985a) *Cell 42*, 39−50.
Vale, R. D., Schnapp, B. J., Mitchison, T., Steuer, E., Reese, T. S., & Sheetz, M. P. (1985b) *Cell 43*, 623−632.
Yang, J. T., Laymon, R. A., & Goldstein, L. S. (1989) *Cell 56*, 879−889.
Yang, J. T., Saxton, W. M., Stewart, R. J., Raff, E. C., & Goldstein, L. S. B. (1990) *Science 249*, 42−47.
Yphantis, D. A., & Waugh, D. F. (1956) *J. Phys. Chem. 60*, 623−635.
Zamyatnin, A. A. (1972) *Prog. Biophys. Mol. Biol. 24*, 107−123.
Zamyatnin, A. A. (1984) *Annu. Rev. Biophys. Bioeng. 13*, 145−165.

BI9429795